Interfacial Crystalline Structures in Injection Over-Molded Polypropylene and Bond Strength

Bowen Yan, Hong Wu,* Genjie Jiang, Shaoyun Guo,* and Jian Huang

The State Key Laboratory of Polymer Materials Engineering, Polymer Research Institute of Sichuan University, Chengdu 610065, China

ABSTRACT This paper describes interfacial crystalline structures found in injection overmolded polypropylene components and the relationship of these structures to bond strength between the components. The combined effects of the development of hierarchical gradient structures and the particular thermomechanical environment near the interface on the interfacial crystalline structures were investigated in detail by PLM, SEM, DSC, WAXD, and infrared dichroism spectroscopy. The experimental results showed that during molding there was competitive formation of interfacial crystalline structures consisted of "shish-kebab" layer (SKL) and a transcrystalline layers (TCL). Variation in shear stress (controlled by injection pressure and injection speed) plays an important role in the formation of the SKL. The formation of TCL is influenced by the thermal environment, namely melt temperature and mold temperature. Increasing within certain limits, interfacial temperature and the thermal gradient near the interface promotes β-iPP growth. The relationship between interfacial crystalline structures and interfacial bond strength was established by lap shear measurement. The interfacial bond strength is improved by enhancing the formation of TCL, but reduced if SKL predominates.

KEYWORDS: interface • crystalline structure • bond strength • injection overmolding • polypropylene

INTRODUCTION

The interfacial microstructure of a polymer matrix, which is formed at the interface developing from solid−melt to solid−solid by thermomechanical mechanisms, is a polymer science and technology research topic currently attracting great interest. Particularly when semicrystalline polymers are chosen as the matrix, the special crystalline structure near the interface needs to be taken into account because of its effect on the final morphology.

In the past few decades, great attention has been paid to the interfacial crystalline structure of polymer/single-fiber composites. Transcrystallization (TC) is usually obtained near the fiber surface and depends on the both the thermomechanical environment and the nucleating ability of the fibers. These fibers are typically composed of organic or inorganic materials such as glass, carbon, aramid, PP, PET and PTFE (1, 2). In the quiescent state, the heterogeneous nucleating ability of the fiber plays a significant role in the formation of the TC (3). However, shear can induce a transcrystalline-like column structure defined as a "cylindrite" by Varga et al. (4−6), via self-nucleation of the polymer matrix as the fiber is pulled during crystallization process. There is another nucleating mechanism associated with melting or at least partial melting of the organic fiber surface, which has been investigated by Li et al through the introduction of the isotactic polypropylene (iPP) fiber into a homogeneous iPP matrix (7−9).

Besides polymer/one-dimensional fiber composites, the interfacial crystalline structure of two-dimensional sheets has also been widely studied. Li et al. (10, 11) studied one type of epitaxial crystallization, the TC of poly(butylene adipate) (PBA) formed on highly oriented thin film because of its strong nucleating ability. In addition, Naiki et al. (12) have reported that TC of iPP occurred on the surface of talc in the quiescent state.

There is much research on crystalline structures near the interface and on the effect of such structures on interfacial adhesion or bond properties. Cho et al. (13) investigated interfacial crystalline structure resulting from TC when iPP crystallized on a high-surface-energy substrate, discovering that the interface was dominated by spherulites and noting that only a very thin transcrystalline region was observed on a low-surface-energy substrate. The adhesion energy as measured by the asymmetric double cantilever beam (ADCB) test increased strongly with transcrystallinity. At the same time, in the interfacial transcrystalline layer (TCL), the increased proportion of of the β-modification of isotactic polypropylene (β-iPP) had strong reinforcing effect on the adhesion property (14).

However, it is well-known that polymer processing methods such as injection molding and extrusion can influence the formation of an interfacial crystalline structure. As one of the most widely employed methods, injection molding is characterized by high productivity, high degree of automation, and good product dimensional stability. There is however, "fountain" flow (15) during injection molding, which is more complex than the ideal conditions normally considered such as the quiescent state and the shearing cell. Therefore, it is important and necessary to study the inter-

* Corresponding author. E-mail: wh@scu.edu.cn (H.W.); nic7702@scu.edu.cn (S.G.). Tel. & Fax: 86-28-85466077 (H.W.); 86-28-85405135 (S.G.).
Received for review April 22, 2010 and accepted September 23, 2010

DOI: 10.1021/am1003574

facial crystalline structure and its effect on the final properties by examination of specimens produced by practical injection molding.

Much attention has been paid to the hierarchical structures formed perpendicular to the flow direction and the gradient of development along the flow direction (16−23), which results in complex and diverse interfacial crystalline structures in polymer matrix composites (12, 24, 25). By using dynamic packing injection molding to impose oscillatory shear on the melt during solidification stage, Zhong et al. (24) have fabricated an iPP blended with poly(ethylene terephthalate) (PET) microfibrils, which exhibited an oriented "shish-kebab" (SK) crystalline structure (26, 27), especially in the skin layer. This interfacial crystalline structure was different from that formed in the quiescent state, and the distribution of the structure was affected by the presence of hierarchical structures. By using the same method (25), TC of PP on the surface of glass fibers was obtained. Furthermore, the application of oscillatory shear could significantly improve fiber orientation and interfacial adhesion between fibers and the PP matrix. Janeschitz−Kriegl investigated the kinetics of flow induced PP crystallization under processing conditions and found that the growth of aggregates of chain molecules by the action of flow after being oriented in the flow direction can lead to threadlike precursors initiating SK structures (28).

In addition to the above-mentioned interfaces, one type of interface obtained during injection molding has attracted great interest in recent years. This novel injection molding technology called injection overmolding (IOM), which is similar to in-mold decorative molding, sequential injection molding and film insert molding, and has been applied in many fields of polymer processing due to significant advantages such as the direct production of soft molded grips to provide comfort to users, structural requirements, complex geometries, elimination of postmolding processes and cost reduction. IOM can be used as a thermal welding technology to carry out welding polymer parts during injection molding. As the interfacial morphology formed during IOM can be controlled artificially and the interface plays a critical role in determining the final properties and hence the reliability of products, it has been the subject of much research. Interface reactions have been studied during sequential injection molding to observe interface reinforcement between a variety of rigid polymers and soft elastomers (29−31). It is also to be expected that using IOM, the final product properties are dependent on the interfacial crystalline structures of the component semicrystalline polymers. Qiu et al. (32) have investigated the effect of interfacial morphologies resulting from controlled variation of IOM processing conditions on the weld or adhesion strength of injection molding polyamide-6 (PA6). It was shown that the zone of TC grew perpendicularly from the interface, which improved the weld strength of the interface. Similarly, Aurrekoetxea et al. (33) have studied the effect of the processing conditions on the bond strength when iPP was injection molded onto a solid PP substrate, indicating that the interfacial strength was largely improved if the interface temperature was higher than the melting temperature of the substrate. In addition, Leong et al. (34−36) have reported that the interfacial adhesion between PP film and PP matrix was evidently increased with increasing barrel temperature and injection holding pressure, and the interfacial crystalline structure was the decisive factor controlling interfacial mechanical properties.

As complex crystalline structures can be formed because of the development of a gradient of hierarchical morphological structures during conventional injection molding, the combined effects of the gradient development of the hierarchical structures and the particular thermomechanical environment near the interface during IOM should result in a range of diverse interfacial crystalline structures. However, the relative study has not been reported yet. In this work, thermomechanical environmental factors, such as melt temperature, mold temperature, injection pressure, and injection speed are controlled to investigate the formation of diverse interfacial crystalline structures and the morphological development during IOM. In addition, a formation mechanism for these diverse interfacial crystalline structures is proposed. The relationship between interfacial crystalline structures and interfacial bond strength is established to enable the control of product properties.

EXPERIMENTAL SECTION

Material. A commercial grade of isotactic polypropylene (iPP) F401 with density of 0.9 g/cm^3 and a melt flow index of 2.5 g/10 min (230 °C/2.16 kg), was supplied by LanZhou Petrochemical Co., China. The onset melting temperature is 155 °C and the maximum melting temperature is 165 °C by using DSC (Q20, TA Instruments Co., U.S.) at a constant heating rate of 10 °C/min.

Specimen Preparation. The injection overmolded specimens were made using a conventional injection molding machine (K-TEC40, Ferromatik Milacron Co., Europe) and a special mold with temperature control system designed in our laboratory. As shown in Figure 1, at the first stage of the injection molding cycle (A), iPP was injected under constant molding conditions into the empty half-cavity to prepare the first molded part. The mold was then opened to clear out the runner scraps and remove the first molded part for cooling to room temperature (25 ± 2 °C). In the second stage (B), the rotary joint was rotated 180°, the first molded part was inserted into the secondary cavity, and the second injection was completed to make the complete molded specimen. The dimensions of the specimen are shown in Figure 1C and the molding conditions for the experimental design and the specimen numbers are summarized in Table 1.

Polarized Light Microscope (PLM). Twenty-micrometer-thick samples were cut by using a microtome (YD-2508, Yidi Medical Appliance Co., China) in directions perpendicular and along the flow. A standard cutting pattern was used to produce seven specimens from each molding (Figure 2) and the cutting procedure numbers are summarized in Table 2. "FD", "ND", and "TD" represent "flow direction", "Normal direction" and "Transverse direction", respectively. "N", "M", and "F" represent the position "near the gate", "in the middle", and "far from the gate", respectively. "S" and "C" represent "skin layer" and "core Layer", respectively. The thin slices were sandwiched between two microscope cover glasses and placed on the microscope stage. The interfacial crystalline structures formed during IOM were observed by using a transmission polarizing light micro-

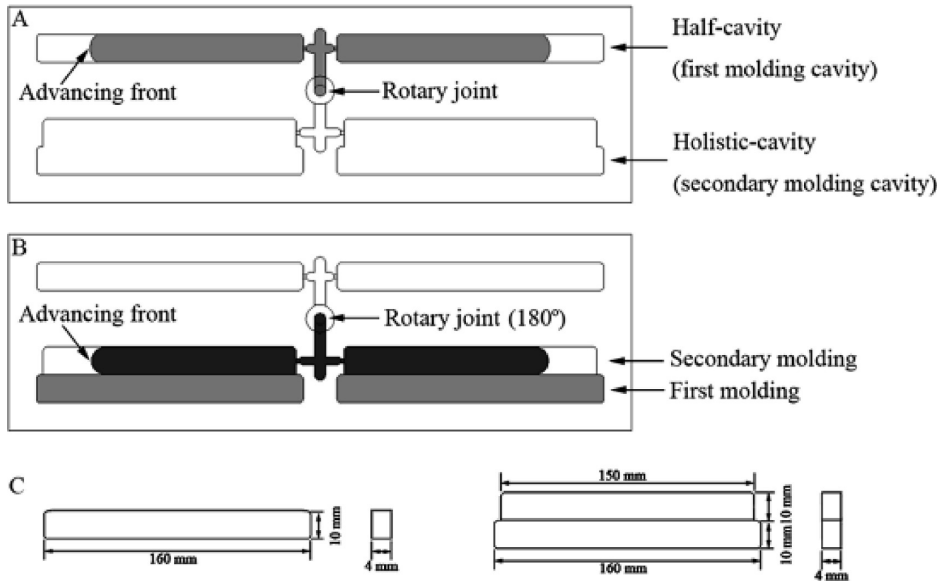

FIGURE 1. (A, B) Schematic representation of the IOM procedure in one mold and (C) the dimensions of the first molded part and the complete molded specimen.

Table 1. Molding Conditions for First and Secondary Moldings[a]

specimen no.[b]	melt temperature (°C)	mold temperature (°C)	injection pressure (MPa)	injection speed (mm/s)
A	210	40	60	40
B1/B2	210/250	60	60	40
C1/C2	210/250	40	60	40
D1/D2	210/250	120	60	40
E1/E2	210/250	140	60	40
F1/F2	210	60	40/80	40
G1/G2	210	60	40/80	80

[a] For all specimens: injection time, 4 s; holding pressure, 20 MPa; holding time, 10 s; cooling time, 10 s. [b] A is the first molding condition; the numbers from B1 to G2 are the secondary molding conditions.

scope (PLM) (12POLS, Leica Co., Germany). Attention was focused on the crystalline structures at the interface between the component parts of the molding.

The β-iPP formed near the interface was investigated on a PLM (DMIP, Leica Co., Germany) equipped with a hot stage (THMS 600, Linkam Co., U.K.). The slice was heated to 130 °C and held for 2 min to achieve thermal equilibrium. Subsequently, it was heated to 175 °C at a constant rate of 1 °C/min. The process of crystal melting was recorded by taking photomicrographs at appropriate intervals by using a digital camera (POWER SHOT 550, Canon Co., Japan).

Scanning Electron Microscope (SEM). The microtomed specimens, were etched with a solution (37) prepared by mixing two parts of sulfuric acid (98%) (Sichuan Xilong Chemical Co., Ltd., China) with one part of phosphoric acid (85%) (Sichuan Xilong Chemical Co., Ltd., China). The etching reagent was then made by dissolving 1 wt % potassium permanganate (Chongqing Boyi Chemical Co., Ltd., China) into the above solvent mixture. After etching, the specimens were washed with distilled water. The surfaces of all the specimens were sputter-coated with a thin layer of gold to provide enhanced conductivity. Then the crystalline structures were observed by a scanning electron microscope (SEM) (XL30FEG, Philips Co., Netherlands) under an acceleration voltage of 10 kV.

Infrared Dichroism Spectroscopy. The orientation distribution in samples taken near the interface was measured using FT-Infrared dichroism spectroscopy (MFT-2000, JASCO, Japan) according to Herman's orientation function (38)

$$f = \frac{R-1}{R+2} \times \frac{2\cot^2\alpha + 2}{2\cot^2\alpha - 1}, R = A_{||}/A_{\perp} \qquad (1)$$

where R is the dichroic ratio defined as the ratio between the absorbance of infrared radiation polarized along directions parallel and perpendicular to the direction of orientation (the direction of flow); α is the angle between the chain axis and the transition moment vector. Approximately 10 μm sections were microtomed along the flow direction for IR scans. The 998 cm^{-1} absorption band with $\alpha = 18°$ was chosen to characterize the crystalline phase orientation (39).

Differential Scanning Calorimetry (DSC) Analysis. To prove the existence of β crystals in injection overmolded PP under different melt and mold temperatures, we cut a film with a thickness of 25 μm from the interface. The resulting films were analyzed by a TA-Q20 (TA Instruments-Waters LLC, USA) thermal system purged with nitrogen. The program for DSC measurement was run from 25 to 220 °C, as the first heating scan. After the sample was equilibrated at 220 °C for 5 min to erase previous thermal and stress history, it was cooled to 25 °C, and then heated again to 250 °C for a second heating scan. All scans were carried out at the rate of 10 °C/min, and the endothermic curves were recorded.

Wide-Angle X-ray Diffractometry (WAXD) Analysis. The same films as used in DSC were analyzed using a Philips X'pert Pro MPD wide-angle X-ray diffractometer (Philips, Netherlands), using Cu Kα X-rays with a voltage of 40 kV and a current of 20 mA. The samples were scanned with 2θ values ranged from 5 to 45°, at a scanning speed of 2°/min.

Lap Shear Measurement for Interfacial Bond Strength. The interfacial bond strength of the specimen was investigated by using lap shear measurement (32, 33, 40) as shown in Figure 3. Two notches were machined from both surfaces to the interface leaving a limited bonding interface length of 10 mm ± 0.5 mm, producing samples with closely controlled bonding interface areas. The samples were examined under various shear conditions. Bond strength was measured on a universal

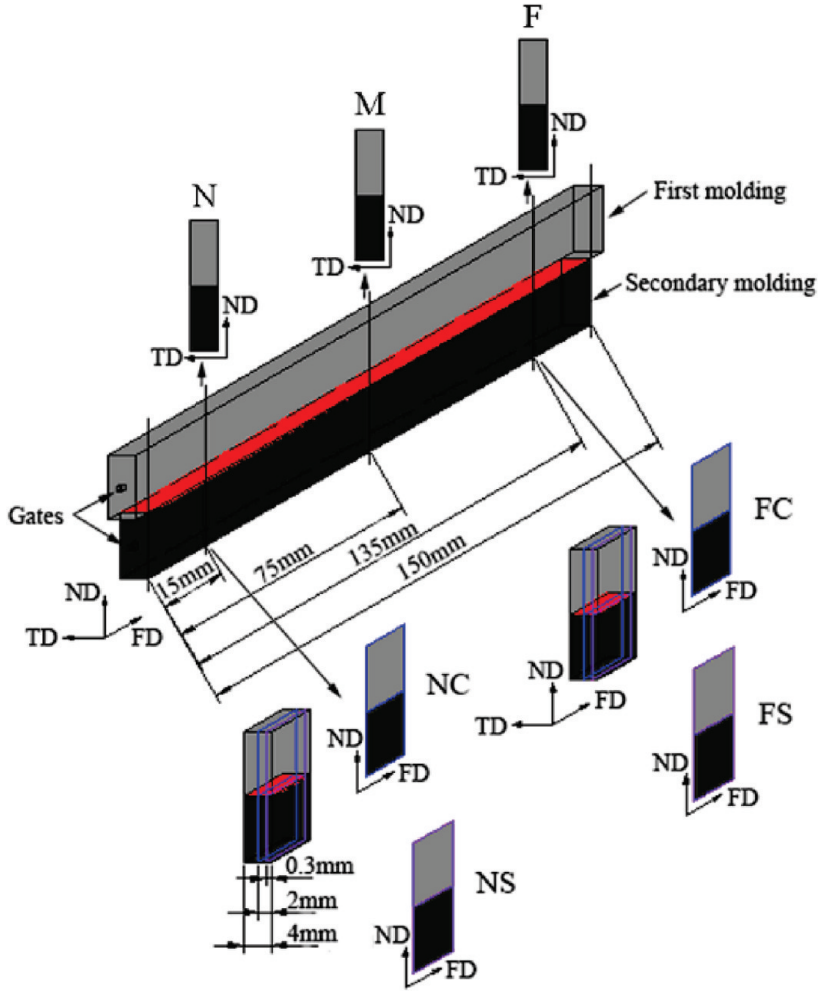

FIGURE 2. Schematic representation of the sample cutting pattern.

Table 2. Specimen Cutting Procedures

procedure numbers	perpendicular to the flow direction (TD × ND)[a]	along the flow direction (FD × ND)[a]	distance from the gate (mm)	distance from the surface (mm)
N	+	−	15	
M	+	−	75	
F	+	−	135	
NS	−	+	15	0.3
NC	−	+	15	2
FS	−	+	135	0.3
FC	−	+	135	2

[a] +, cutting along the direction indicated; − no cut made.

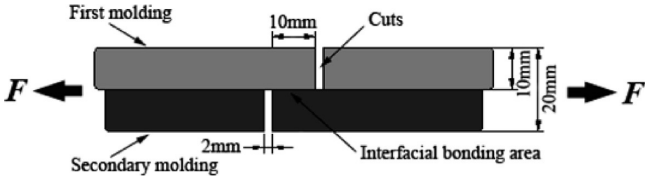

FIGURE 3. Dimensions of specimen for the lap shear measurement.

materials testing machine (CMT-4104, ShenZhen SANS Testing Machine Co., China) operating in tension mode with a crosshead speed of 10 mm/min at 23 °C ± 2 °C. The shear strength was calculated by the maximal load divided by the area of the bonding interface (10 × 4 mm^2) and the given values of strength were calculated as the average over 10 specimens.

RESULTS AND DISCUSSION

1. Interfacial Morphology Development. ***1.1. Morphology Perpendicular to the Flow Direction.*** Figure 4 shows the optical micrographs near the interface, which were prepared under secondary molding conditions (B1) and the cutting procedures N, M, and F. It can be clearly observed that a bright region and a black region develop gradually on the interface at different distances from the gate. The area of the bright region expands and the black region gradually disappears with distance from the gate, so that only bright region remains at the interface at 135 mm from the gate (F). More evident interfacial crystalline structures can be found in the micrographs from two rectangular regions: the interfacial region near the surface of the specimens along TD is defined as region 1 (R1) and the center of the interface is defined as region 2 (R2). The development of two different morphologies can be seen by comparing R1 with R2. One is the TCL growing perpendicular to the interfacial direction in R1 (N, M and F) and R2 (F). The other is the black region, which is hard to find in the structure by examining the PLM micrographs in R2 (N and M).

1.2. Morphology along the Flow Direction. The optical micrographs taken near the interface along the flow direction were obtained under the same molding conditions

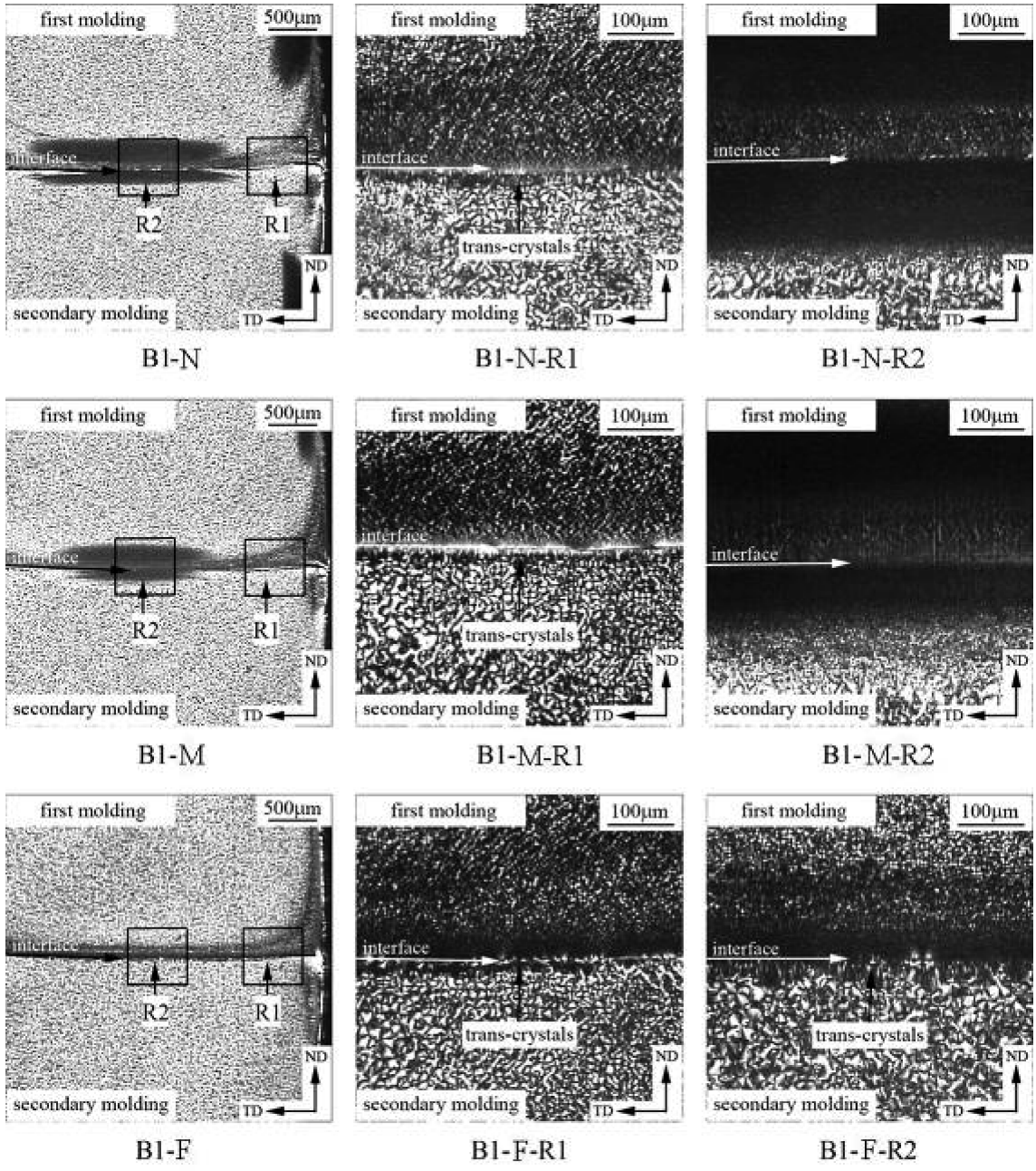

FIGURE 4. Polarized optical micrographs near the interface at different distances from the gate perpendicular to the flow direction (the secondary molding condition B1 and the cutting procedures N, M, and F. Melt temperature = 210 °C, mold temperature = 60 °C.)

(B1), as shown in Figure 5. The uniform development of the interfacial morphology is shown by examination of samples taken at different distances from the gate and the surface. Along the flow direction, there is always TCL growing perpendicular to the interfacial direction near the surface of the specimens, i.e., the direction perpendicular to R1 (from NS to FS). Note that the morphology develops from the black region to the TCL in the center of the interface, i.e., the direction perpendicular to R2 (from NC to FC). However, it can be clearly seen that the large SK structures can be observed near the interface along the flow direction (NS), but this structure cannot be found in the other optical micrographs (NC, FS, and FC).

Figure 6 shows SEM micrographs of etched samples taken near the interface at different distances from the gate and the same distance from the surface (the center of the interface) along the flow direction, i.e., corresponding to Figure 5 (B1-NC and B1-FC). There are many very small SK structures growing along the flow direction on the interface in Figure 6 (NC' and NC"), differing from the black region shown in Figure 5 (NC). It is difficult to find any structure in the black region because of the low magnification of PLM and the intensive shish-kebab structures. From Figure 6 (FC' and FC"), it is clearly shown that the interfacial crystalline structures are uniform as those presented in Figure 5 (FC). It is further shown that the TCL grows perpendicular to the interfacial direction far from the gate.

2. Effect of Temperature on Interfacial Morphology. Figure 7 shows the effects of melt temperature and

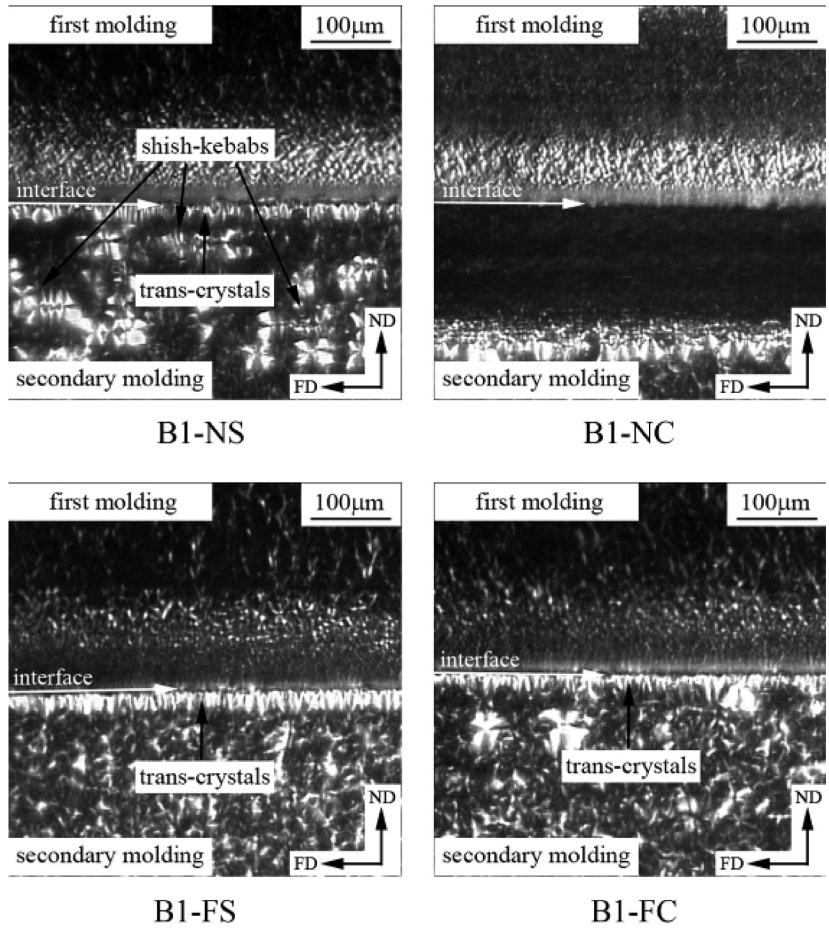

FIGURE 5. Polarized optical micrographs near the interface at different distances from the gate and the surface along the flow direction (the secondary molding condition B1 and the cutting procedures NS, NC, FS, and FC. Melt temperature = 210 °C, Mold temperature = 60 °C.)

mold temperature on the interfacial crystalline structures at different distances from the gate and perpendicular to the flow direction (N, M, and F). The interfacial crystalline structures at low melt temperature (210 °C) are apparently different from that at high melt temperature (250 °C). The SK layer (SKL) is more readily developed at low melt temperatures, vanishing at high melt temperatures comparing C1, D1 with C2, D2. When a high melt temperature is used, only TCL is observed in the whole range of the interface at different mold temperatures. It can be seen by comparing C1 to D1 that an increase in mold temperature generally results in the shrinkage of the SKL. It is beneficial to the properties of the product to expand the TCL and reduce the SKL by increasing melt and mold temperatures. At the same time, the effect of the melt temperature on the interfacial crystalline structures is more significant than that of the mold temperature. In addition, the interfacial crystalline structures far from the gate (F) are only composed of TCL, while the SKL cannot be found in this region even over a range of melt and mold temperatures.

To show more detail of the interfacial crystalline structures, magnified optical micrographs taken in different regions (R1 and R2) are shown in Figure 8. These images were obtained at different melt and mold temperatures, but at the same distance from the gate perpendicular to the flow direction. There are two different features of the interfacial crystalline structures from B1 to E2. First, the thickness of the TCL gradually increases with raising melt and mold temperatures, which also increases the dimensions of spherulites observed near the interface of the secondary molded part. Second, variation in thermal environment (composed of melt and mold temperatures) leads to the formation of diverse interfacial crystalline structures, so that the birefringence of the TCL shown in Figure 8 (D2 and E2) differs significantly from the others. From other studies (5−11), the fan-shaped crystalline structures with strong birefringence are the TCL of β-iPP, indicated by arrows. Figure 9 depicts the effect of thermal environment on the thickness of the TCL. The thickness gradually increases with the increasing melt and mold temperatures. Furthermore, the thickness in R2 is wider than that in R1 at the same interface perpendicular to the flow direction. This due to the slower cooling rate, i.e., a higher crystalline temperature in R2 than that in R1.

3. Effect of Shear Stress on Interfacial Morphology. Figure 10 shows the effects of injection pressure and injection speed on the interfacial crystalline structures at different distances from the gate perpendicular to the flow direction. The wide SKL (black region) can be obtained under high injection pressure (F2 and G2), whereas there is no significant effect on the interfacial crystalline structures

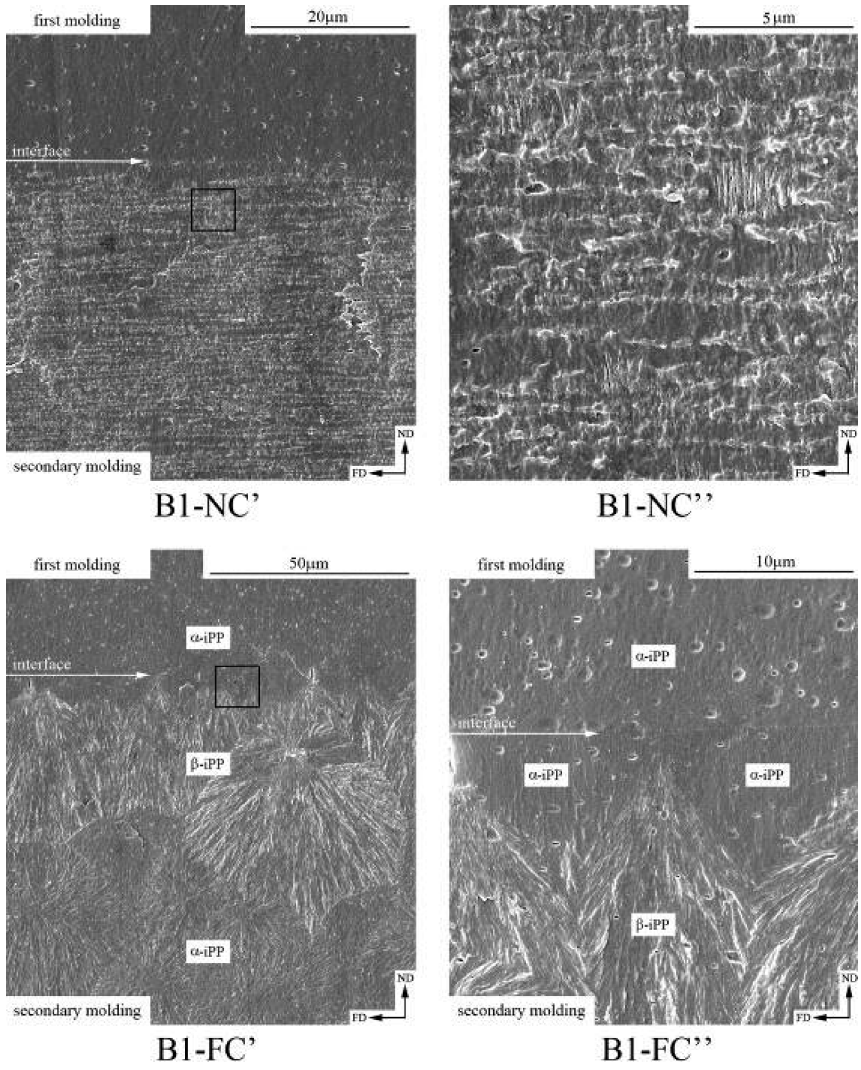

FIGURE 6. SEM micrographs near the interface at different distances from the gate and the same distance from the surface (NC and FC) along the flow direction (the secondary molding condition B1. Melt temperature = 210 °C, mold temperature = 60 °C.)

achieved by changing the injection speed from 40 to 80 mm/s. From the micrographs, the TCL can be found on the interface under different molding conditions in the same region (R1). At the same time, if the injection pressure remains high (80 MPa), the SKL gradually expands with increasing injection speed as indicated by arrows in R1 (comparing F2-N-R1 with G2-N-R1). However, the SKL cannot be formed by changing the injection speed in this region when a low injection pressure is used (F1-N-R1 and G1-N-R1). However, the thickness of the TCL has a slight decrease from 18.3 to 16.4 μm when increasing the injection pressure (to 40 MPa) and the injection speed to 40 mm/s. It is concluded that the shear stress (controlled by injection pressure and injection speed) has a positive effect on the formation of the SKL and acts to reduce the thickness of the TCL.

4. Formation Mechanism of Diverse Interfacial Crystalline Structures. ***4.1. Competing Interfacial Morphology.*** As shown in Figures 4−6, the SKL and the TCL, compete to form the interfacial morphology during IOM. To understand the morphology development and the resulting diverse interfacial crystalline structures more clearly, we proposed a three-dimensional model (Figure 11). It proposes distribution and evolution rules for the interfacial crystalline structures. During IOM, the complex thermomechanical environment results in different degrees of orientation of the molecular chains perpendicular to and along the flow direction, and hence diverse interfacial crystalline structures are formed in various regions (i.e., R1 and R2 perpendicular to the flow direction) of different interfaces (i.e., I and II along the flow direction). At different regions of every interface, the orientation degree in R2 is higher than that in R1 as a result of "fountain" flow during the molding process, i.e., the flowing melt more readily contacts the surface of the first molded part in R2, so that the forms preferentially SKL in R2. However, the shear stress decreases along the flow direction so that the orientation degree gradually reduces. Therefore, the interface I (i.e., near the gate) is dominated by the SKL.

4.2. Interfacial "Shish-Kebab" Layer (SKL). There is a significant difference between IOM and conventional injection molding in that the shish-kebab structures can be formed on the interface during IOM, as shown in Figure 6 (B1-NC'). To show the difference more clearly, an

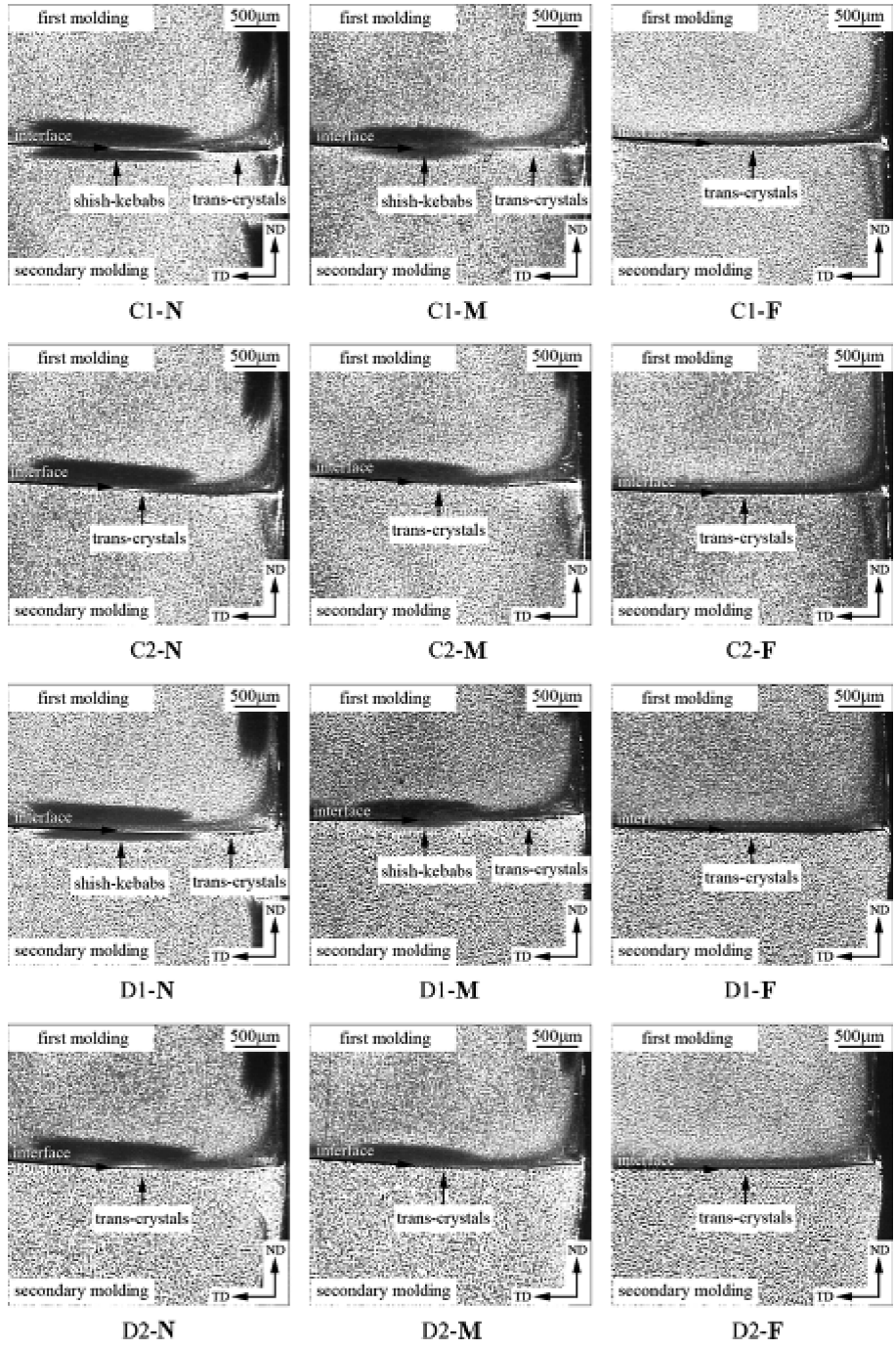

FIGURE 7. Polarized optical micrographs near the interface prepared by different melt temperature and mold temperature at different distances from the gate perpendicular to the flow direction (the secondary molding conditions C1, C2, D1, and D2 and the cutting procedures N, M, and F. Sample C1: melt temperature = 210 °C, mold temperature = 40 °C. Sample C2: melt temperature = 250 °C, mold temperature = 40 °C. Sample D1: melt temperature = 210 °C, mold temperature = 120 °C. Sample D2: melt temperature = 250 °C, mold temperature = 120 °C).

overall low magnification view is shown in Figure 12. It can be seen that the shish-kebab structures develop in the subskin layer during conventional injection molding, i.e., in the subskin layer of the first molded part for IOM. In addition, the skin layer of the first molded part has no visible structure, which has been reported as a "structureless" skin layer by Kantz et al (41). However, the shish-kebab structures are formed on the interface during IOM, i.e., in the skin layer of the secondary molded part. During conventional injection molding, the SKL can be formed due to enhanced orientation degree of molecular chains under high shear at the subskin layer, which exists between the freezing skin layer and the flowing melt (42−44). However during IOM, high shear can be induced on the interface between the solid surface of the first molded part and the melt of the secondary molding since the surface of the first molded part is similar to the skin layer in conventional injection molding.

Although the shish-kebab structures are formed in different layers during IOM and conventional injection molding, their formation mechanism is the same. For IOM, the shear stress, governed by injection pressure and injection speed, plays an important role in the flow induced orientation of

FIGURE 8. Optical micrographs near the interface obtained at different melt temperature and mold temperature at the same distance from the gate perpendicular to the flow direction (the secondary molding conditions B1, B2, C1, C2, D1, D2, E1, and E2, the cutting procedure M).

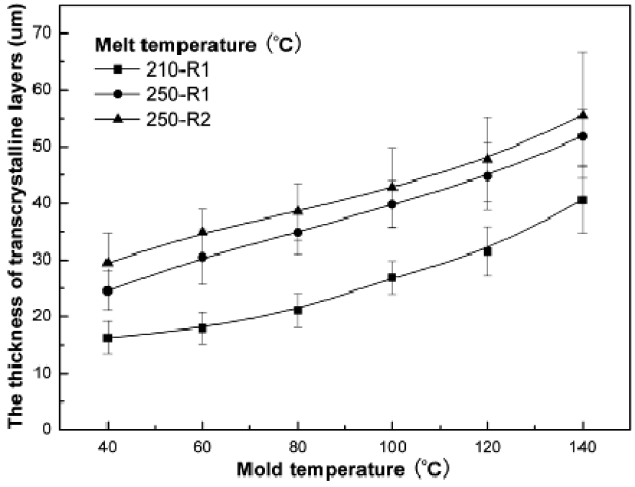

FIGURE 9. Effects of melt temperature and mold temperature on the thickness of the TCL in different regions (R1 and R2).

molecular chains and the relaxation time before crystallization. High shear stress results in enhanced molecular orientation and a short time for relaxation to occur, thus a thick and wide SKL is formed. However, thermal environment, which is controlled by melt and mold temperatures, diminishes the effect of the time for relaxation. Furthermore, the increased melt temperature, which can decrease the characteristic relaxation time of the molecular chains and prolong the time for the relaxation, is more significant than increased mold temperature, which can only prolong the time for the relaxation.

Orientation distributions of crystalline phase of injection overmolded PP near the interface measured by FT-infrared Dichroism Spectroscopy are shown in Figure 13. It is found that the orientation at the skin layer (<50 μm) is much higher than that at subskin layer, indicating that the SKL is possibly formed in the skin layer during the molding process. However, the SKL is usually formed in the subskin layer because the orientation at subskin layer is much higher than that at skin layer during conventional injection molding. However, a higher degree of orientation of the crystalline phase is found under low melt temperature (210 °C) and low mold temperature (40 °C), indicating that the TCL layer is enhanced under such molding conditions. More detailed studies on the orientation of the molecular chains of the diverse interfacial crystalline structures during IOM will be investigated by using 2D WAXS and reported elsewhere.

4.3. Interfacial Transcrystalline Layer (TCL).

The polymer matrix can crystallize on the surface of the substrate as nucleating agent because of a sufficiently high density of nuclei, which will hinder the lateral extension and force growth in one direction resulting in a columnar crystalline layer perpendicular to the interface, known as TCL. So the nature of the surface of the substrate, which exhibits strong nucleating ability toward the melt of polymer matrix, is the necessary condition to the formation of the TCL. During IOM, the surface of the first molded part acts as the substrate so that the formation of TCL becomes possible.

The thermomechanical environment during IOM plays an important role in determining the nucleation and growth of the TC. Thermal stress, shear stress, and the enhanced mobility of molecular chains in the amorphous phase promotes the nucleation of the TC on the surface of the first molded part. First, thermal stress originates from the shrinkage process because the hot melt of the secondary molding

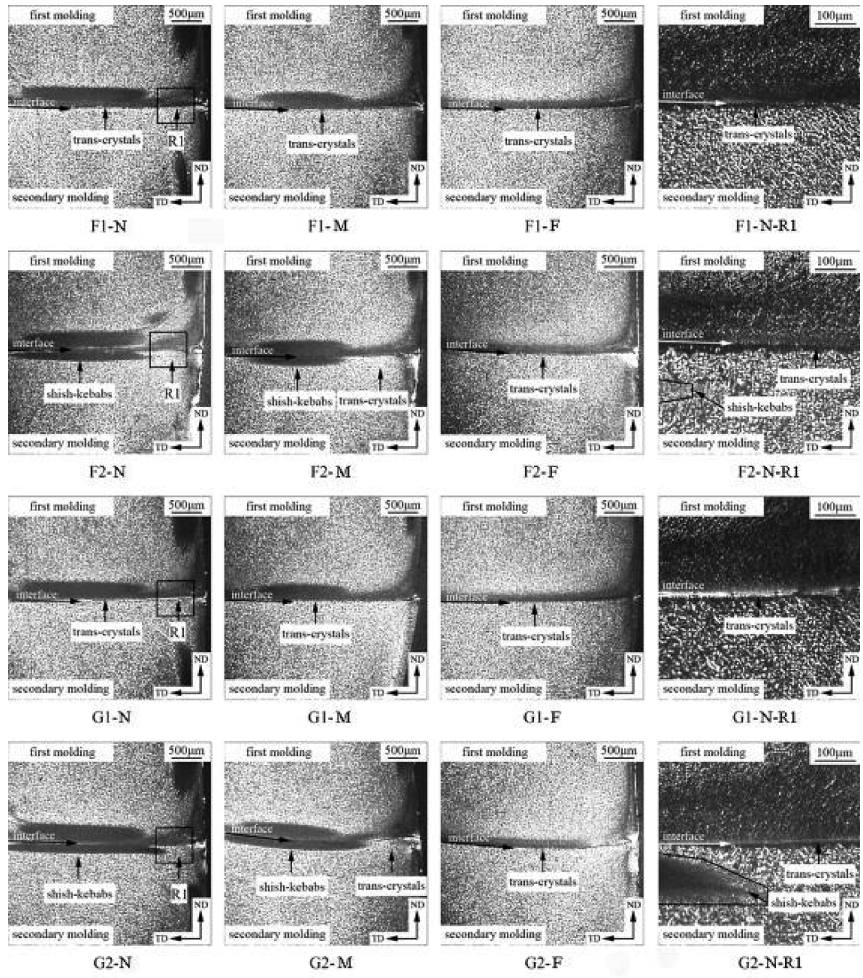

FIGURE 10. Polarized optical micrographs near the interface prepared by different injection pressure and injection speed at different distances from the gate perpendicular to the flow direction (the secondary molding conditions F1, F2, G1, and G2 and the cutting procedures N, M, and F. Sample F1: injection pressure = 40 MPa, injection speed = 40 mm/s. Sample F2: injection pressure = 80 MPa, injection speed = 40 mm/s. Sample G1: injection pressure = 40 MPa, injection speed = 80 mm/s. Sample G2: injection pressure = 80 MPa, injection speed = 80 mm/s. All of samples: melt temperature = 210 °C, mold temperature = 60 °C).

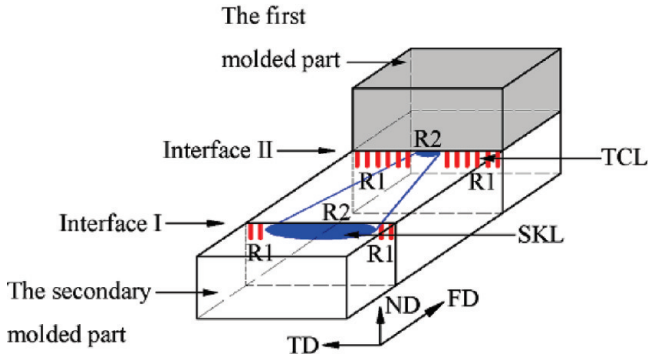

FIGURE 11. Schematic representation of the morphology development and the diverse interfacial crystalline structures at different regions of different interfaces during IOM.

contacts the cold (room temperature) solid surface of the first molded part. Second, shear stress is initiated by shear between the flowing melt of the secondary molding and the solid surface of the first molded part. Third, the mobility of molecular chains in amorphous phase at the surface of the first molded part can be enhanced by increasing the interfacial temperature (T_i), which is determined by the initial contact temperature between the solid surface of the first molded part and the melt of the secondary molding. In this work, the surface temperature of the first molded part (T_1) remains at room temperature (25 °C), whereas the melt temperature of the secondary molding (T_2) is controlled artificially. So T_i can be estimated from $T_i = (T_1 + T_2)/2$ (27, 30, 45), the relevant data are listed in Table 3 (T_2 is assumed to be constant in the mold during IOM). It is concluded that the crystalline phase at the surface of the first molded part is not molten because the onset melting temperature of the iPP is near 155 °C which is above T_i. Therefore, these three different effects result in a drop of crystallization stearic hindrance on the interface so that high-density nucleation can be induced on the interface. However, the increased crystallization time resulting from increased melt and mold temperatures can promote the growth of the TCL.

It is interesting to note that the interfacial crystalline structures such as β-iPP were found in some molding conditions during IOM, such as in locations far from the gate, as shown in Figure 6 (FC′ and FC″) and under conditions of high melt and mold temperatures as shown in Figure 8 (D2 and E2). Figure 14 shows that the optical characteristics change

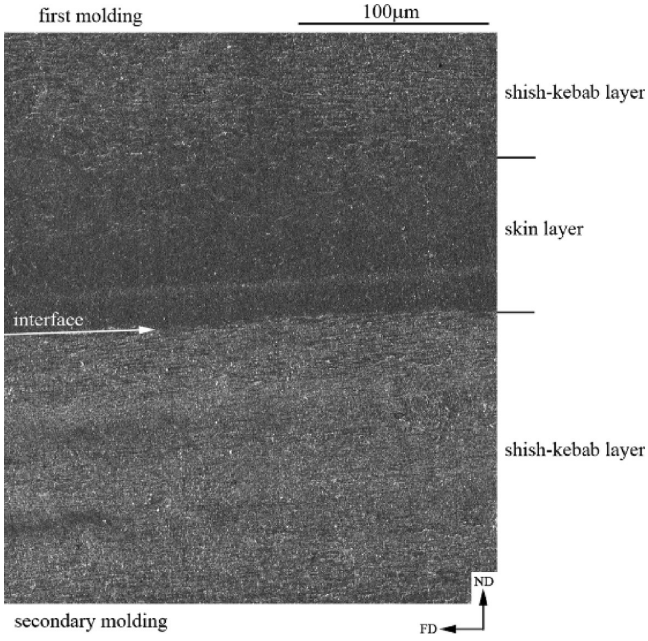

FIGURE 12. SEM micrographs of the different morphologies in the first molded part and the secondary molded part obtained by conventional injection molding and IOM respectively along the flow direction and near the gate (the secondary molding condition B1 and the cutting procedure NC. Sample B1: melt temperature = 210 °C, mold temperature = 60 °C).

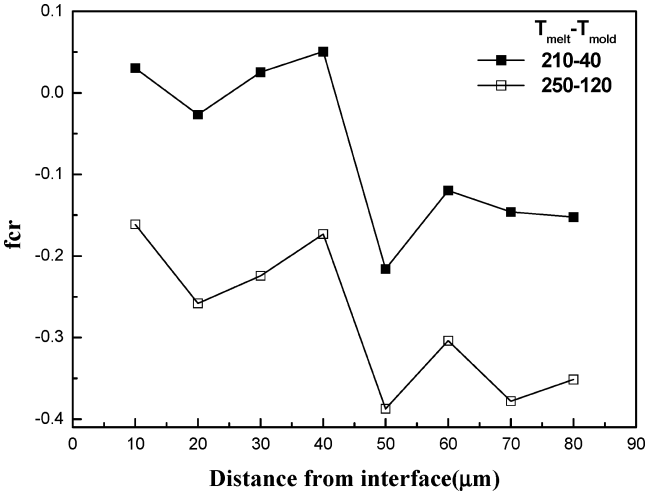

FIGURE 13. Orientation distributions at the surface of crystalline phase (fcr) in over injection molded PP under different melt and mold temperature.

Table 3. Temperature Parameters of the Interface

melt temperature T_2 (°C)	interfacial temperature T_i (°C)	thermal gradient $\Delta T = T_2 - T_i$ (°C)
210	117.5	92.5
250	137.5	112.5

from a strong birefringence to a negative, and then back to a strong birefringence again, and finally the optical characteristics disappear gradually when the temperature rises above the melting temperature at a constant heating rate of 1 °C/min. The melting test demonstrates that observed fan-shaped crystalline structure with strong birefringence is the metastable β-iPP.

Many investigations have reported that β-iPP is metastable and can be formed under special conditions, such as high thermal gradient, shearing or elongation of the melt, and the addition of β-nucleating agents (4−9, 14, 46). During IOM, the complex nonisothermal gradient, which is dependent on melt and mold temperatures, is the most important factor for the formation of the β-iPP. Varga et al. (4−6) reported that the linear growth rate of the β-iPP from the melt was higher than that of the α-iPP within the temperature range of $T_{\alpha\beta}$ (α to β transition) ≈ 100 °C and $T_{\beta\alpha}$ (β to α transition) ≈ 140 °C, but it was lower than that of the α-iPP outside of this temperature range. Furthermore, β-iPP was readily formed under high thermal gradients (46). As shown in Table 3, the thermal gradient near the interface ($\square T$) is related to T_i and T_2. T_i was limited in the range of 100 to 140 °C, in which the growth rate of β-iPP was faster than that of the α-iPP, so that β-iPP readily began to grow along the oriented α-iPP front as shown in Figures 6 and 8. When T_1 is fixed, the increased mold temperature can only extend the time for crystallization but does not affect T_i. However, the increased melt temperature not only has the same effect of extending the time for crystallization but also can increase T_i and $\square T$ as shown in Table 3, which form a suitable temperature range for the growth of the β-iPP. It can be demonstrated the use of DSC to produce melting curves (Figure 15) and WAXD Patterns (Figure 16) that the production of β crystals from injection overmolded PP was enhanced at the interface under high melt temperatures (250 °C) and high mold temperature (120 °C) because the endothermic peak at lower temperatures (147 and 152 °C) and the enhanced β crystalline peak were found in the DSC and WAXD curves. However, note that the effect of shearing and elongation of the melt on the formation of the β-iPP during IOM has not been examined in this work.

5. Relationship between the Interfacial Crystalline Structures and Bond Strength. The formation of the interfacial crystalline structures determines the interfacial mechanical properties of IOM moldings, specifically the interfacial bond strength. Figure 17 shows the effects of melt and mold temperatures on the interfacial bond strength assessed by lap shear measurement. The interfacial bond strength increases gradually with increasing melt and mold temperatures. The maximal bond strength (17.5 MPa) can be obtained at the highest melt and mold temperatures. Observed fracture positions are not along the interface when the melt temperature was 250 °C and the mold temperature was above 120 °C. As shown in Figures 7 and 8, certain diverse crystalline structures are the decisive factor for changing the interfacial bond strength. With the increased thickness of the TCL, the interfacial bond strength will gradually increase. Conversely, the bond strength will become worse with the enlargement of the SKL.

The relationship between the competing interfacial morphologies and the interfacial bond strength should be understood, so that the bond strength can be predicted from the development of interfacial morphologies and that this development can be controlled by varying the molding

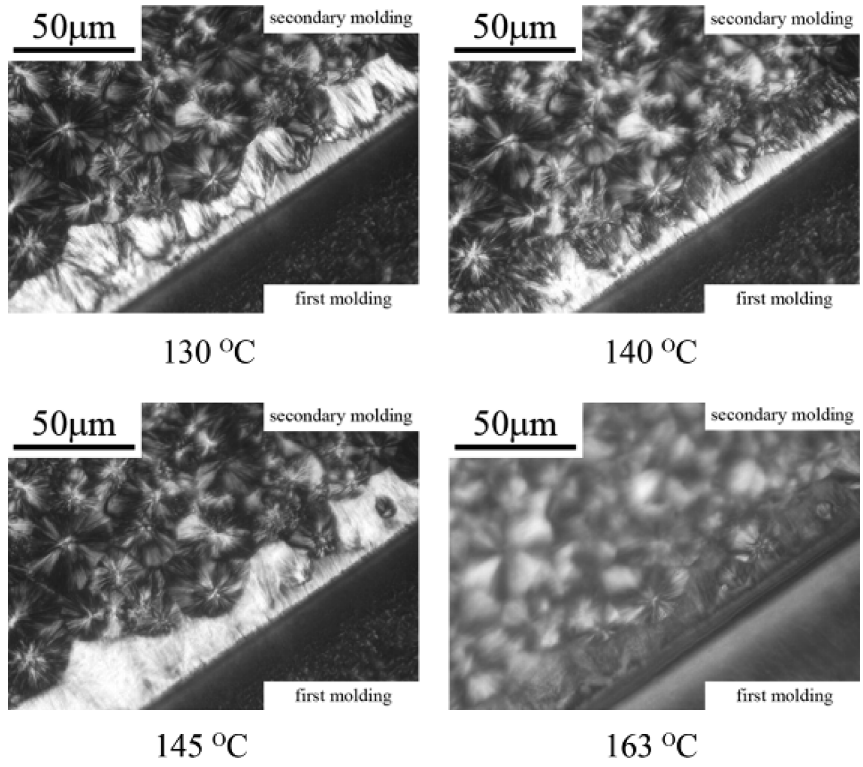

FIGURE 14. Melting test by using PLM equipped with a hot stage at a constant heating rate of 1 °C/min.

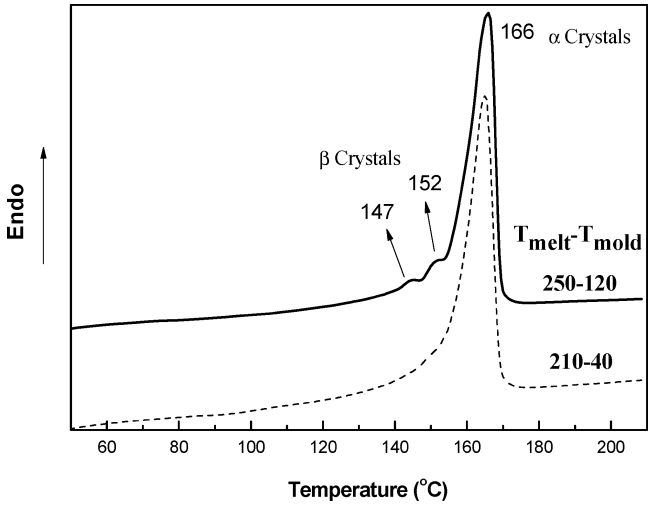

FIGURE 15. DSC melting curves of over injection molded PP under different melt and mold temperatures.

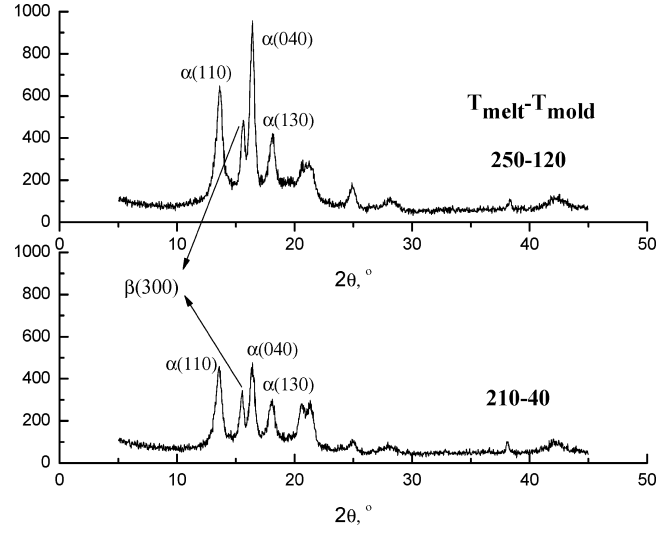

FIGURE 16. WAXD patterns of over injection molded PP under different melt and mold temperatures.

conditions. First, increasing temperature gives better interfacial bond strength. Second, the interfacial bond strength decreases under high injection pressure and injection speed. Similar conclusions have been obtained from work using PET film as the first molded part and other PET as the secondary molding during film insert molding (33). Third, the interfacial bond strength far from the gate is improved more significantly than that near the gate.

To verify the relationship between interfacial crystalline structure and the bond strength, we have designed three different kinds of interfaces (A, B, and C) by controlling the thermomechanical processing environment (i.e., molding conditions) listed in Table 4. Figure 18 shows the interfacial bond strength determined by using lap shear measurement

Table 4. Molding Conditions for Three Different Types of Interfaces (A, B, and C)[a]

sample numbers	melt temperature (°C)	mold temperature (°C)	injection pressure (MPa)	injection speed (mm/s)
A	190	25	80	80
B	230	80	40	30
C	250	120	40	30

[a] For all specimens: injection time, 4 s; holding pressure, 20 MPa; holding time, 10 s; cooling time, 10 s.

and the fracture modes, which represent three distinct fracture surfaces corresponding to three different kinds of interface. Sample A fractures easily along the interfacial direction without any plastic deformation and its maximum

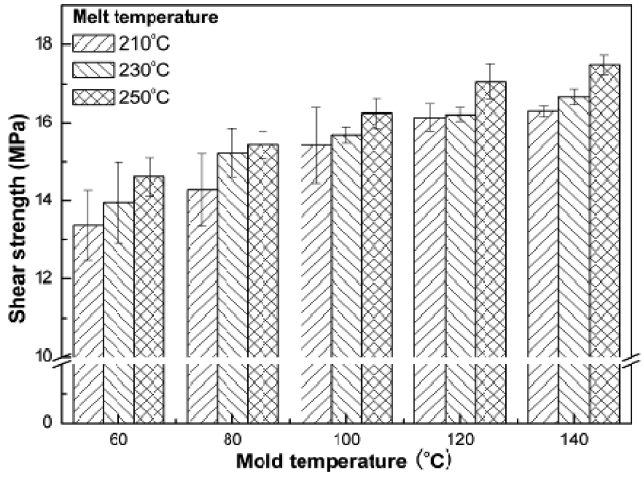

FIGURE 17. Effects of melt temperature and mold temperature on interfacial bond strength by using lap shear measurement.

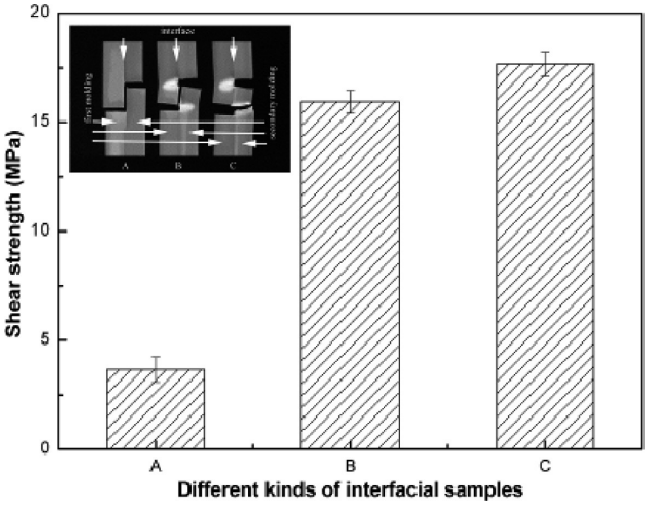

FIGURE 18. The bond strength by using lap shear measurement and the fracture modes of the three different types of interfaces.

shear strength is 3.5 MPa. This is due to the extensive SKL on the interface resulting from low melt and mold temperatures and high shear stress. However, TCL still develops in the region far from the gate, which leads to heterogeneous morphology over the whole interface. Nevertheless, there is a significant increase in the shear strength for sample B and sample C, which improve by 357 and 406 % compared to sample A. At the same time, there is a highly significant difference between samples B and C: the stress whitening present near the cutting and the fracture along interfacial direction is seen in sample B, whereas the fracture direction of sample C is not along the interfacial direction, indicating that the bond strength of the interface is higher than that of the substrate, due to the formation of the homogeneous TCL on the interface. Moreover, the bond strength will be increased further with the enhanced thickness of the TCL resulting from rising melt and mold temperatures.

Figure 19 shows the fracture surfaces of the secondary molded part for sample A and sample B, but the surface of sample C cannot be observed by using the same method since the fracture did not occur along the interfacial direction. The fracture surfaces obtained by lap shear measurement at the same crosshead speed rate, were smooth (sample A) and rough (sample B). Moreover, the SEM micrographs in Figure 19 show the different regions corresponding to the above-mentioned R1 and R2, as shown in Figure 4. The strong interfacial bond results from distinct plastic deformation occurring in R1 for sample B (B-R1). Similarly, there is little deformation for sample A at the same region (A-R1). In A-R2, the smooth fracture surface reveals that there is no significant effect on the bond strength for sample A due to the formation of the SKL along the flow direction on the interface. However, distinct plastic deformation is found (as shown in B-R2) which indicates that the thickness of the TCL in R2 is greater than that of the R1 depicted in Figure 9.

CONCLUSIONS

For IOM, the diverse interfacial crystalline structures, which consisted of competing SKL and TCL morphologies,

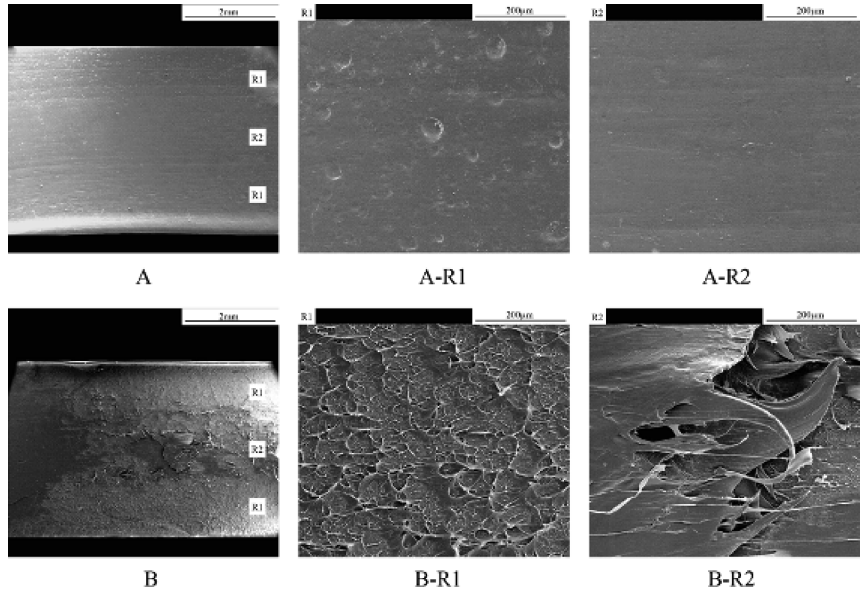

FIGURE 19. SEM micrographs of the fracture surfaces of the secondary molded part (the secondary molding conditions A and B).

formed at different regions (perpendicular to the flow direction) of different interfaces (along the flow direction). The interfacial morphology developed from the SKL to the TCL along the flow direction. At the same time, the SKL more readily formed in region 2 (R2) and the TCL was more readily obtained in region 1 (R1) perpendicular to the flow direction. The thermomechanical environment (controlled by varying molding conditions) played a significant role in the development of the interfacial morphology and the formation of the diverse interfacial crystalline structures. The thermal environment (melt and mold temperature) had a positive effect on the formation of the TCL. However, the SKL could be obtained under high shear stress controlled by injection pressure and injection speed. In addition, the SKL typically formed in the position near the gate, whereas the TCL generated more readily further from the gate.

It was significantly that the shish-kebab structures could be formed on the interface during IOM but in the subskin layer during conventional injection molding. The formation of the SKL was ascribed to high shear stress resulted from enhanced orientation of molecular chains and short relaxation time for before crystallization. However, the nucleation of the TC was influenced by thermal stress, shear stress, and the enhanced mobility of molecular chains in amorphous phase. For the TCL, the increased interfacial temperature and the increased thermal gradient near the interface could promote β-iPP growth at a suitable temperature range.

The formation of the TCL could significantly improve the interfacial bond strength, but the existence of SKL reduces it, so the thermal environment enhances the interfacial bond strength, whereas high stress reduces it. We have shown this by detailed examination of three different types of interfaces obtained by controlling the thermomechanical environment by means of processing conditions.

Acknowledgment. Financial support from the National Natural Science Foundation of China (50703027) and the Special Funds for Major State Basic Research Projects of China (2005CB623800) are gratefully acknowledged.

REFERENCES AND NOTES

(1) Wang, C.; Liu, C. R. *Polymer* **1999**, *40*, 289–298.
(2) Thomason, J. L.; Van Rooyen, A. A. *J. Mater. Sci. Lett.* **1992**, *27*, 897–907.
(3) Wang, C.; Hwanc, L. M. *J. Polym. Sci., Part B: Polym. Phys.* **1996**, *34*, 47–56.
(4) Varga, J.; Karger-Kocsis, J. *J. Polym. Sci., Part B: Polym. Phys.* **1996**, *34*, 657–670.
(5) Varga, J.; Karger-Kocsis, J. *Polymer* **1995**, *36*, 4877–4881.
(6) Wu, C. M.; Chen, M.; Karger-Kocsis, J. *Polymer* **1999**, *40*, 4195–4203.
(7) Li, H.; Jiang, S.; Wang, J.; Wang, D.; Yan, S. *Macromolecules* **2003**, *36*, 2802–2807.
(8) Li, H.; Zhang, X.; Duan, Y.; Wang, D.; Li, L.; Yan, S. *Polymer* **2004**, *45*, 8059–8065.
(9) Li, H.; Zhang, X.; Kuang, X.; Wang, J.; Wang, D.; Li, L.; Yan, S. *Macromolecules* **2004**, *37*, 2847–2853.
(10) Sun, Y.; Li, H.; Huang, Y.; Chen, E.; Zhao, L.; Gan, Z.; Yan, S. *Macromolecules* **2005**, *38*, 2739–2743.
(11) Liu, J.; Wang, J.; Li, H.; Shen, D.; Zhang, J.; Ozaki, Y.; Yan, S. *J Phys Chem B* **2006**, *110*, 738–742.
(12) Naiki, M.; Fukui, Y.; Matsumura, T.; Nomura, T.; Matsuda, M. *J. Appl. Polym. Sci.* **2001**, *79*, 1693–1703.
(13) Cho, K.; Kim, D.; Yoon, S. *Macromolecules* **2003**, *36*, 7652–7660.
(14) Boucher, E.; Folkers, J. P.; Creton, C.; Hervet, H.; Leger, L. *Macromolecules* **1997**, *30*, 2102–2109.
(15) Tadmor, Z. *J. Appl. Polym. Sci.* **1974**, *18*, 1753–1772.
(16) Tan, V.; Kamal, M. R. *J. Appl. Polym. Sci.* **1978**, *22*, 2341–2355.
(17) Strebel, J. J.; Mirabella, F.; Blythe, C.; Pham., T. *Polym. Eng. Sci.* **2004**, *44*, 1588–1593.
(18) Pantani, R.; Coccorullo, I.; Speranza, V.; Titomanlio, G. *Polymer* **2007**, *48*, 2778–2790.
(19) Wenig, W.; Stolzenberger, C. *J. Mater. Sci.* **1996**, *31*, 2487–2493.
(20) Kalay, G.; Bevis, M. J. *J. Polym. Sci., Part B: Polym. Phys.* **1997**, *35*, 265–291.
(21) Yu, X. F.; Wu, H.; Li, J.; Guo, S. Y.; Qiu, J. H. *Polym. Eng. Sci.* **2009**, *49*, 703–712.
(22) Viana, J. C.; Cunha, A. M.; Billon, N. *Polymer* **2002**, *43*, 4185–4196.
(23) Viana, J. C. *Polymer* **2004**, *45*, 993–1005.
(24) Zhong, G. J.; Li, Z. M.; Li, L. B.; Shen, K. Z. *Polymer* **2008**, *49*, 4271–4278.
(25) Wang, K.; Guo, M.; Zhao, D. G.; Zhang, Q.; Du, R. N.; Fu, Q.; Dong, X.; Han, C. C. *Polymer* **2006**, *47*, 8374–8379.
(26) Seki, M.; Thurman, D. W.; Oberhauser, J. P.; Kornfield, J. A. *Macromolecules* **2002**, *35*, 2583–2594.
(27) Janeschitz-Kriegl, H. *Macromolecules* **2006**, *39*, 4448–4454.
(28) Janeschitz-Kriegl, H.; Ratajski, Ewa *Polymer* **2005**, *46*, 3856–3870.
(29) Jiang, G, J,; Wu, H.; Yan, B. W.; Guo, S. Y.; Huang, J. *J. Polym. Sci., Part B: Polym. Phys.* **2009**, *47*, 1112–1124.
(30) Carella, A. R.; Alonso, C.; Merino, J. C.; Pastor, J. M. *Polym. Eng. Sci.* **2002**, *42*, 2172–2181.
(31) Arzondo, L. M.; Pino, N.; Carella, J. M.; Pastor, J. M.; Merino, J. C.; Poveda, J.; Alonso, C. *Polym. Eng. Sci.* **2004**, *44*, 2110–2116.
(32) Qiu, J. H.; Tsuboi, A.; Izumi, K.; Wu, H.; Guo, S. Y.; Huang, Y. D. *Polym. Eng. Sci.* **2007**, *47*, 2164–2171.
(33) Aurrekoetxea, J.; Gastillo, G.; Cortes, F.; Sarrionandia, M. A.; Urrtibeascoa, I. *J. Appl. Polym. Sci.* **2006**, *102*, 261–265.
(34) Leong, Y. W.; Yamaguchi, S.; Mizoguchi, M.; Hamada, H.; Ishiaku, U. S.; Tsujii, T. *Polym. Eng. Sci.* **2004**, *44*, 2327–2334.
(35) Yamaguchi, S.; Leong, Y. W.; Tsujii, T.; Mizoguchi, M.; Ishiaku, U. S.; Hamada, H. *J. Appl. Polym. Sci.* **2005**, *98*, 294–301.
(36) Leong, Y. W.; Hamada, H. *Int Polym Proc* **2008**, *2*, 183–191.
(37) Olley, R. H.; Bassett, D. C. *Polymer* **1982**, *23*, 1707–1712.
(38) Samuels, R. J. *Makromol. Chem.* **1981**, *4*, 241–270.
(39) Samuels, R. J. *Polym. Eng. Sci.* **1988**, *28*, 852–856.
(40) Yang, F.; Pitchumani, R. *Macromolecules* **2002**, *35*, 3213–3224.
(41) Kantz, M. R.; Newman, J. R.; Stigale, F. H. *J. Appl. Polym. Sci.* **1972**, *16*, 1249–1260.
(42) Tadmor, Z. *J. Appl. Polym. Sci.* **1974**, *18*, 1753–1772.
(43) Fleischmann, E.; Zipper, P.; Janosi, A.; Geymayer, W.; Koppelmann, J.; Schurz, J. *Polym. Eng. Sci.* **1989**, *29*, 835–843.
(44) Zipper, P.; Janosi, A.; Geymayer, W.; Ingolic, E.; Fleischmann, E. *Polym. Eng. Sci.* **1996**, *36*, 467–482.
(45) Smith, G. D.; Plummer, C. J. G.; Bourban, P.; Manson, J. E. *Polymer* **2001**, *42*, 6247–6257.
(46) Lovinger, A. J.; Chua, J. O.; Gryte, C. C. *J. Polym. Sci., Part B: Polym. Phys.* **1977**, *15*, 641–656.

AM1003574